Comparison of Functional Domains in Vertebrate-Type Ferredoxins†

Milka Kostic,‡ Susan Sondej Pochapsky,‡ John Obenauer,§,|| Huaping Mo,‡,⊥ Gina M. Pagani,§ Robert Pejchal,§,# and Thomas C. Pochapsky*,‡

Departments of Chemistry and Biochemistry, Brandeis University, Waltham, Massachusetts 02454-9110

Received January 9, 2002; Revised Manuscript Received March 14, 2002

ABSTRACT: The vertebrate-type $Cys_4Fe_2S_2$ ferredoxins are a class of small acidic proteins that typically act as electron shuttles between NAD(P)H-dependent reductases and monoxygenases, particularly cytochromes P450. Nuclear magnetic resonance assignments and detailed analysis of nuclear Overhauser effects permit the direct comparison of the functional C-terminal domains of three vertebrate-type ferredoxins, the mammalian adrenodoxin (Adx) and the bacterial ferredoxins putidaredoxin (Pdx) and terpredoxin (Tdx). In particular, homologous hydrogen-bonding networks involving a conserved basic residue (His 49 in Pdx, His 56 in Adx, Arg 49 in Tdx) are detailed. This hydrogen bond network appears to play a role in the mechanical transmission of redox-dependent conformational and dynamic changes from the iron−sulfur binding loop to the C-terminal domain. Hydrogen/deuterium exchange measurements have been made in Adx as a function of oxidation state for comparison with previous studies of Pdx and Tdx. The results of these measurements highlight the importance of the conserved basic residue in the linkage between oxidation state and protein dynamics. Finally, a series of mutations have been made in the C-terminal domain of Pdx, including one, Y51F, that disrupts the proposed hydrogen-bonding network without perturbing steric and hydrophobic interactions in the functional domain. Although the mutant is considerably destabilized with respect to wild-type Pdx, relatively unperturbed chemical shifts for residues near the site of the mutation and NOEs between water and Phe 51 suggest that the network is reconstituted with a solvent water in place of the tyrosine hydroxyl group in this mutant.

The $Cys_4Fe_2S_2$ ferredoxins are a family of small (80−130 residues) redox-active proteins that function as electron transfer agents in many biological redox processes, including photosynthesis, respiration, and oxidative metabolism. Members of the family are found in virtually every living organism and act as single electron shuttles, cycling between Fe(II)/Fe(III) and Fe(III)/Fe(III) oxidation states at the metal cluster. They exhibit a range of reduction potentials that appear to be modulated primarily by hydrogen bonding from backbone and side chain groups to the metal cluster sulfur atoms, although solvent accessibility and the number of charged residues around the cluster are also likely to affect reduction potentials (*1*, *2*).

Most of the $Cys_4Fe_2S_2$ ferredoxins that have been structurally characterized to date exhibit the same folding topology as ubiquitin. These structures are conveniently considered as consisting of two "lobes" with most of the N-terminal half of the polypeptide sequence concentrated in one lobe and the C-terminal half in the other. The iron−sulfur cluster binding site is situated at one end of the molecule between the N- and C-terminal lobes (see Figure 1). The N-terminal lobe contains the conserved hydrophobic core and adopts approximately the same structure in all of the ferredoxins characterized to date, that is, a mixed four-stranded β-sheet and a long α-helix that crosses the β-strands approximately perpendicularly. This is the so-called ubiquitin superfold or β-grasp motif (*3*). Although some insertions/deletions are observed in loop and turn regions of the N-terminal lobes across the $Cys_4Fe_2S_2$ ferredoxin family, the number of residues making up the conserved core N-terminal structure is constant at about 36 amino acid residues, not including the iron−sulfur binding loop. It should be noted that the iron−sulfur cluster binding loop (which contains three of the four cysteinyl ligands for the metal cluster) is usually somewhat longer (by three residues) in the vertebrate-type ferredoxins than in the plant ferredoxins. This may be related to the requirement for redox-dependent conformational shifts in the vertebrate-type ferredoxins (vide infra) (*4*).

Unlike the N-terminal lobes, the C-terminal lobes of $Cys_4Fe_2S_2$ ferredoxins show considerable variability, both in polypepide length and in tertiary structure. This is particularly obvious when plant-type (chloroplast) ferredoxins are compared with vertebrate-type ferredoxins. The plant-type ferredoxins generally have shorter C-terminal peptides (35−45 residues) and show relatively little well-defined secondary structure in the C-terminal lobe (*5*−*10*). The C-terminal lobes of vertebrate-type ferredoxins typically contain more residues than do the plant-type proteins (between 50 and 70 residues) and contain more regular secondary structure, as well. All of the structurally characterized vertebrate-type ferredoxins

† This work was supported by a grant from the National Institutes of Health (GM44191 to T.C.P.).

* To whom correspondence should be addressed. E-mail: pochapsk@brandeis.edu. Phone: 781-736-2559. Fax: 781-736-2516. Website: http://www.chem.brandeis.edu/pochapsky.

‡ Department of Chemistry, Brandeis University.

§ Department of Biochemistry, Brandeis University.

|| Current address: Department of Biology, Massachusetts Institute of Technology, Cambridge, MA.

⊥ Current address: Eli Lilly Corp., Indianapolis, IN.

Current address: Department of Biochemistry, University of Michigan, Ann Arbor, MI.

10.1021/bi0200256 CCC: $22.00
Published on Web 04/17/2002

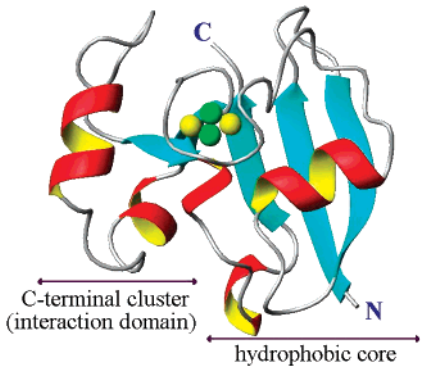

FIGURE 1: Ribbon representation of the crystallographic structure of Adx^o (*11*). The two domains of vertebrate-type ferredoxins, the hydrophobic core (N-terminal lobe), and the C-terminal cluster are shown, with the Fe_2S_2 cluster positioned between them. The N-terminal lobe, containing the hydrophobic core, is structurally conserved throughout the Fe_2S_2 ferredoxin family. All figures of protein structure were made using MOLMOL (*67*).

have one long and one short α-helix in the C-terminal lobe, a well-defined β-sheet that is continuous with the large β-sheet of the N-terminal lobe, and at least one β-turn (Figure 1). Vertebrate-type ferredoxins for which structures have been determined include adrenodoxin (Adx)[1] (*11*, *12*), putidaredoxin (Pdx) (*13*, *14*), terpredoxin (Tdx) (*15*), and *Escherichia coli* ferredoxin (Fdx) (*16*).

With the exception of the *E. coli* ferredoxin, for which a precise function has not yet been determined (*17*), all of the structurally characterized vertebrate-type ferredoxins are associated with oxidative metabolism and act as electron shuttles between cytochromes P450 and NAD(P)H-dependent reductases. Adx functions as a reductant for the mammalian P450 isozymes involved in selective oxidation of cholesterol to form pregnenolone and the biosynthesis of cortisol and aldosterone, CYP11A1, CYP11B1, and CYP11B2, respectively (*18*). Putidaredoxin (Pdx) is the physiological reductant and effector for cytochrome $P450_{cam}$ (CYP101) in the camphor hydroxylase system from *Pseudomonas putida*. CYP101 catalyzes the 5-*exo*-hydroxylation of camphor by molecular oxygen in the first step in camphor metabolism (*19*). Terpredoxin (Tdx) functions in the same role in the metabolism of terpineol by *Pseudomonas*, shuttling electrons to cytochrome $P450_{terp}$ (CYP108) (*20*, *21*). For all of these reactions, two electrons are required for each turnover of the monooxygenase, requiring two discrete binding and electron transfer events per turnover.

The interactions between ferredoxin and cytochrome in these systems appear to be quite specific. Adx and Tdx exhibit little or no cross-reactivity with CYP101. Bovine Adx is capable of transferring the first electron to CYP101, but substrate turnover is not observed in the camphor hydroxylase system reconstituted with Adx replacing Pdx (*22*). Although Tdx is a *Pseudomonas* ferredoxin, it exhibits no more than 2% of the activity of Pdx in the reconstituted camphor monooxygenase system (H. Gong and T. C. Pochapsky, unpublished results). As a result, it has been concluded that the determinants of molecular recognition in these systems are specific amino acid residues on the surfaces of the cognate ferredoxin/P450 pairings. A considerable amount of mutagenesis data now exists to support the role of specific amino acids in the formation of complexes between the vertebrate-type ferredoxins and their cognate P450 enzymes (*23*−*29*). We have proposed a structure-based model for the specific interactions between Pdx and CYP101 that has received both experimental and theoretical support from work in other laboratories (*30*−*32*).

It is worth noting that all of the residues that have been implicated thus far in interactions between the vertebrate-type ferredoxins and their cognate redox partners are located either on the Fe_2S_2 binding loop or in the C-terminal lobe. As such, the C-terminal lobes of Pdx, Adx, and Tdx are sometimes called "interaction domains". For convenience, we will continue to refer to the interaction domain as the C-terminal lobe throughout this paper. Despite the high degree of specificity inherent in ferredoxin-P450 interactions, many structural similarities exist between the C-terminal lobes of these three proteins, and these common features appear to be linked to the biological function of these proteins. In particular, it has been noted that the residue immediately following the third cysteinyl ligand in the iron−sulfur cluster binding loop (Cys 48 in Pdx, Cys 55 in Adx) is a conserved basic residue, usually a histidine (His 56 in Adx, His 49 in Pdx). Occasionally, as in Tdx, this residue is an arginine (Arg 49). In all of the vertebrate-type ferredoxin structures determined thus far, this conserved basic residue is central to a network of hydrogen bonds that extend throughout the C-terminal lobe. Figure 2 details the hydrogen bond network as determined from the truncated bovine adrenodoxin structure (*11*). Via this network, the conserved His (Arg) has been proposed to act as a mechanical link between the metal cluster binding loop and the C-terminal lobe, transmitting redox-dependent conformational and dynamic perturbations between the metal cluster and the interaction domain (the C-terminal lobe) (*4*, *11*). In Adx, a hydrogen bond is formed between the $O_\gamma H$ hydroxyl proton of Ser 88 and the unprotonated $N_{\epsilon 2}$ of His 56. The $N_{\delta 1}H$ proton of His 56 hydrogen bonds to the backbone carbonyl oxygen of Tyr 82 (*11*). In Pdx, instead of a direct hydrogen bond between Ser 82 $O_\gamma H$ (which is homologous to Ser 88 in Adx) and His 49 $N_{\epsilon 2}$, the $O_\eta H$ of Tyr 51 forms an intermediate set of hydrogen bonds, accepting the $O_\gamma H$ proton of Ser 82 and bonding through its own $O_\eta H$ proton to the $N_{\epsilon 2}$ of His 49. The situation in Tdx differs from both Adx and Pdx, in that Tdx appears to use a salt bridge as one of the primary interactions with residue 49 (vide infra). Herein, we provide a detailed comparison of the C-terminal domains of Adx, Pdx, and Tdx using nuclear magnetic resonance (NMR) and site-directed mutagenesis methods. We interpret these structural observations in light of differences in sensitivity of the three proteins to changes in oxidation state, stability, and function.

[1] Abbreviations: Adx, adrenodoxin; Adx^o, oxidized adrenodoxin; Adx^r, reduced adrenodoxin; CYP101, cytochrome $P450_{cam}$; DTT, dithiothreitol; HSQC, heteronuclear single-quantum correlation; IPTG, isopropyl β-thiogalactoside; LB, Luria−Bertani media; MALDI-TOF, matrix-assisted laser desorption ionization−time of flight mass spectrometry; NMR, nuclear magnetic resonance; NOE, nuclear Overhauser effect; NOESY, NOE spectroscopy; OD, optical density; Pdx, putidaredoxin; Pdx^o, oxidized putidaredoxin; Pdx^r, reduced putidaredoxin; rmsd, root mean square deviation; Tdx, terpredoxin; TOCSY, total correlation spectroscopy; TPPI, time-proportional phase incrementation; WT, wild type; PCR, polymerase chain reaction; 2D, two dimensional; 3D, three dimensional.

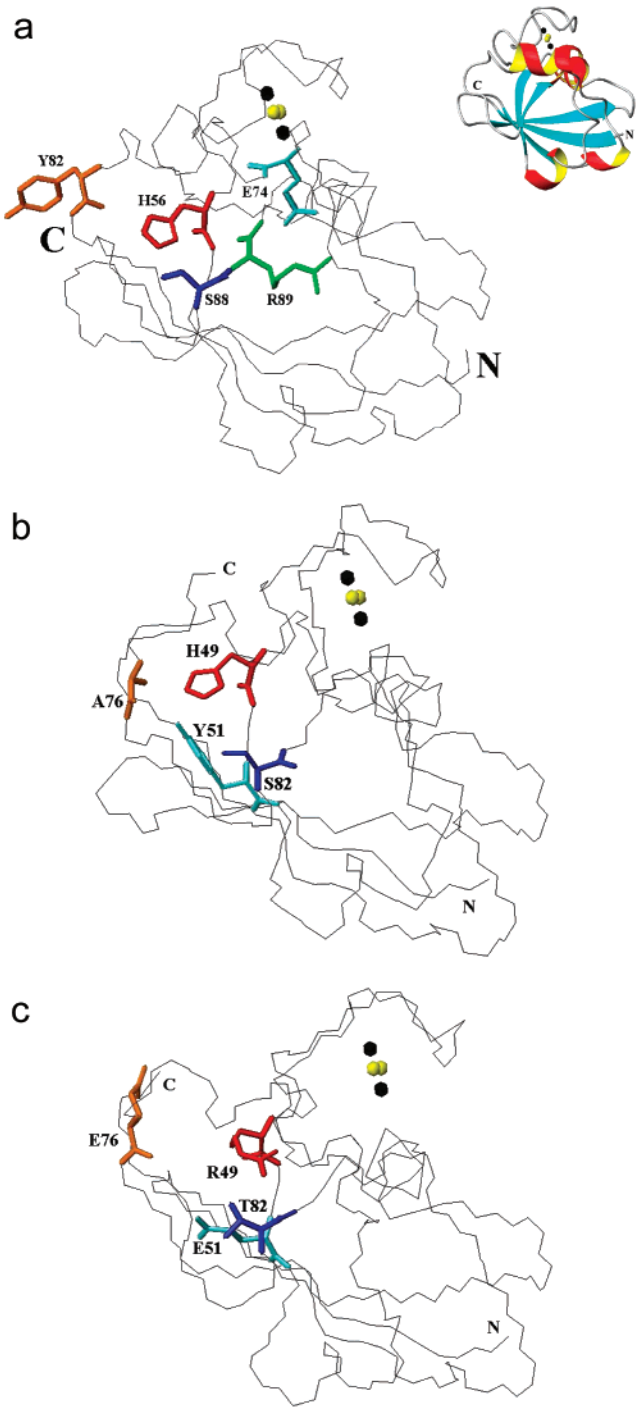

FIGURE 2: (a) Backbone representation of the Adx^o structure (*11*). Side chains of residues proposed to be involved in the hydrogen-bonding network (His 56, Tyr 82, and Ser 88) as well those forming a conserved salt bridge (Glu 76 and Arg 89) are represented and labeled. The iron−sulfur cluster is shown as four spheres (black = Fe; yellow = S). The inset is a ribbon representation of the Adx structure in the same orientation. (b) Backbone representation of the solution structure of Pdx^o (*14*). Side chains of residues proposed to be involved in the hydrogen-bonding network (His 49, Tyr 51, Ser 82, and Ala 76) are represented. The iron−sulfur cluster is shown as four spheres. The orientation of the structure is the same as the orientation of Adx in panel a. (c) Backbone representation of the solution structure of Tdx^o (*15*). Side chains of residues proposed to be involved in the hydrogen-bonding/salt bridge network, Arg 49, Glu 51, Thr 82, and Glu 76, are represented. The iron−sulfur cluster is shown as four spheres. The orientation of the structure is the same as the orientation of Adx in panel a.

MATERIALS AND METHODS

Construction of a Synthetic Human Adx Gene and Expression System. An expressible gene encoding for a truncated human Adx (4−114) was synthesized de novo using a convergent oligonucleotide method. A complete description of the gene synthesis, including oligonucleotides used, is available as Supporting Information. The truncated Adx construct was chosen on the basis of previously published results indicating that the full-length bovine protein is sensitive to protease activity and purification often resulted in obtaining heterogeneous mixtures, with polypeptides that were of variable lengths at the C-terminus. Also, the crystal structure of full-length bovine Adx^o revealed that residues beyond 112 are not observed in the structure (*12*) and that backbone NMR assignments of oxidized full-length human Adx could not be made for residues 115−128 (*33*), both indications of disorder at the C-terminus. On the other hand, bovine Adx (4−114) shows increased resistance toward proteases, with stability and physical and biological properties matching those of WT Adx (*34*).

The sequence of WT human Adx is shown in Figure 3, with the points of truncation used in the current construct indicated. The sequence of the synthetic gene is optimized for *E. coli* expression and incorporates an *Nde*I restriction site at the initiator Met codon and a *Bam*HI site after the stop codon for convenient insertion into pET expression plasmids (*35*). The designed DNA sequence is

```
          10         20         30         40         50
CATATGGAAG ACAAAATCAC TGTACACTTC ATCAATCGCG ACGGTGAAAC

          60         70         80         90         100
GTTGACCACC AAAGGTAAAG TTGGTGACTC TCTGCTGGAC GTCGTTGTTG

          110        120        130        140        150
AAAACAATCT AGATATCGAT GGTTTCGGTG CATGCGAAGG TACGCTAGCG

          160        170        180        190        200
TGCTCCACGT GCCACCTGAT CTTCGAAGAC CACATCTACG AAAAACTGGA

          210        220        230        240        250
CGCGATCACC GACGAAGAAA ACGACATGCT AGATCTGGCG TACGGTCTGA

          260        270        280        290        300
CCGACCGGTC GAGACTGGGT TGCCAGATCT GCCTGACCAA ATCCATGGAC

          310        320        330        340
AACATGACCG TTCGTGTTCC GGAAACCGTT GCGGACGCGT AAGGATCC
```

Site-Directed Mutagenesis and Plasmid Construction in Pdx. The H49F, H49R, and Y51F mutations of Pdx were prepared using the four-primer method used previously for other mutations in Pdx. Primers used for the mutagenesis are listed in the Supporting Information (*4*).

Protein Expression, Reconstitution, and Purification. All Pdx, Adx, and Tdx samples used in this work were prepared from protein overexpressed in *E. coli* strain BL21(DE3)-pLysS by induction of T7 RNA polymerase production with IPTG. Construction of appropriate pET-derived plasmid constructs for Pdx and Tdx expression has been described previously (*4*, *15*). Expression and purification of all proteins, including uniformly ^{15}N- and ^{15}N,^{13}C-labeled samples, were also accomplished as described previously. For the highest yields, it was desirable to reconstitute the ferredoxins prior to purification. Reconstitution was performed as described previously (*4*).

In the case of Y51F Pdx, the whole sample preparation except initial lysis and reconstitution was done in a Coy

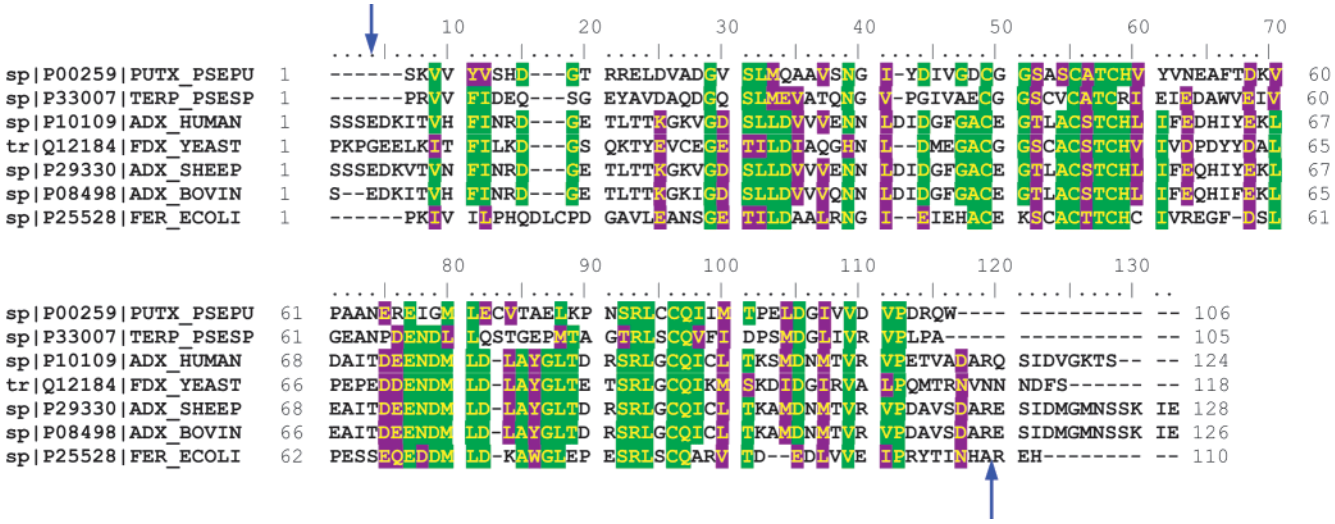

FIGURE 3: Sequence alignment of Pdx, Tdx, human Adx, yeast ferredoxin, sheep and bovine Adx, and ferredoxin from *E. coli*. The alignment was performed using ClastalW (*68*). Conserved residues are highlighted in red and similar residues in green. Arrows mark the position where the human Adx construct used in this work is truncated.

anaerobic chamber under a 5% H_2/95% N_2 atmosphere, at 4 °C, due to the sensitivity of the Y51F mutant to oxygen. Reconstitution of Y51F Pdx was performed under argon at room temperature. MALDI-TOF mass spectrometry was used to confirm the presence of the appropriate mutation. Mass spectra were obtained on a Perseptive Biosystems Voyager TOF mass spectrometer operating in the positive ion mode. Samples were desorbed from a sinapinic acid matrix. Calculated masses are 11407 Da for WT Pdx and 11391 Da for Y51F Pdx. Observed masses were 11413 and 11396 Da for WT and Y51F Pdx, respectively. The calculated mass difference between the WT and the mutant is 16 Da, and a difference of 17 Da is observed. H49R and H49F Pdx could not be reconstituted and purified by standard methods, so the presence of the correct mutation was inferred from the gene sequence rather than mass spectrometry.

Redox Potential Measurements. The redox potentials of Y51F Pdx, human Adx (4−114), and Tdx were measured via the dye photoreduction method, using safranine O (Sigma) as indicator and mediator in this photoinduced reaction, as described elsewhere (*36*). A Shimadzu photodiode array spectrophotometer was used to follow the extent of the reaction. Photoreduction was initiated using a 300 W tungsten lamp. Data were analyzed using the Nernst equation. All redox potential measurements were made at room temperature.

Activity Assays. The activity of Y51F Pdx was determined using the reconstituted camphor monooxygenase enzyme system. The reaction mixture contained 5 μM ferredoxin (WT Pdx was assayed for comparison purposes, together with Y51F Pdx), 0.5 μM each 1 mM putidaredoxin reductase and CYP101, 1 mM camphor, 1 mM DTT, and 330 μM NADH, all prepared in 50 mM Tris-HCl buffer, pH = 7.4. The reaction was followed by measuring the linear decrease of absorbance intensity at 340 nm (NADH consumption) on a Shimadzu photodiode array spectrophotometer. Details of the method have been reported by others (*24*).

NMR Experiments. Ferredoxin samples for all NMR experiments were 1−2 mM in 90/10 H_2O/D_2O, pH 7.4, 50 mM *d*-Tris-HCl, and 1 mM DTT unless otherwise noted. All NMR experiments were performed on either a Varian Unity Inova 500 11.74 T spectrometer or a Varian Unity Inova 600 14 T spectrometer. The Unity Inova 500 operates at 499.706 and 50.68 MHz for ^{1}H and ^{15}N, respectively. The Unity Inova 600 operates at 599.699 and 60.774 MHz for ^{1}H and ^{15}N, respectively. ^{1}H chemical shifts are referenced to external DSS using the ^{1}H resonance of H_2O as internal reference. ^{15}N chemical shifts are referenced to the ^{1}H frequency using a proportionality ratio of 0.101329118 (*37*). Coherence selection in the ^{15}N dimensions of experiments performed on the Unity Inova spectrometers was obtained using pulsed field gradients, and sensitivity enhancement and phase sensitivity were obtained using Rance−Kay acquisition and combinational processing schemes (*38*, *39*). The GARP-1 composite pulse decoupling scheme was used for broad-band decoupling of ^{15}N during acquisition (*40*). All NMR experiments were performed at 17 °C (290.15 K) unless otherwise noted.

A suite of sensitivity-enhanced 3D triple resonance experiments were used in order to make sequence-specific backbone ^{1}H, ^{13}C, and ^{15}N side chain resonance assignments of the 4−114 construct of Adx. These experiments, along with acquisition parameters, are listed in Table 1. All experimental pulse sequences used are standard in Varian ProteinPack release for INOVA spectrometers (Varian, Inc.) and were used as implemented without modification other than parameter optimization. Data were acquired on a Varian Unity Inova 600, equipped with a 5 mm ^{1}H{^{13}C,^{15}N} pulse field gradient probe. As mentioned above, during ^{1}H acquisition, ^{15}N was decoupled using the GARP-1 composite pulse decoupling scheme.

Adx amide H/D exchange in D_2O was measured via a time−course series of ^{1}H−^{15}N HSQC experiments performed on the Unity Inova 500 MHz NMR spectrometer using uniformly ^{15}N-labeled Adx^o and Adx^r, as described previously for Pdx (*41*). Spectral widths were 8082.4 and 1833.3 Hz in ^{1}H and ^{15}N dimensions, respectively. The experiments were carried out using 128 × 1024 complex points, with a total of eight scans per t_1 point. The estimated lag time between the initiation of exchange and the acquisition of the first ^{1}H−^{15}N HSQC experiment was about 30 min, which means that rate constants for processes occurring on a shorter

Table 1: Spectral Parameters for NMR Data Sets Collected on Human Adx^o (4−114)

	d_1 (^{1}H)[a]		d_2			d_3		
experiment[b]	SF (MHz)	SW (Hz)	nucleus	SW (Hz)	N_2[c]	nucleus	SW (Hz)	N_3[c]
2D ^{1}H−^{15}N HSQC	499.71	8082.44	^{15}N	1833.35	128			
2D ^{1}H−^{13}C HSQC	499.71	8082.44	$^{13}C^{aliphatic}$	12565.54	600			
2D ^{1}H−^{13}C HSQC	499.71	8082.44	$^{13}C^{aromatic}$	7539.32	200			
3D HNCO	499.71	8082.44	$^{13}C'$	2500	96	^{15}N	1833.35	32
3D HNCA	499.71	8082.44	$^{13}C^{\alpha}$	3769.74	128	^{15}N	1833.35	32
3D HNCACB	499.71	8082.44	$^{13}C^{\alpha,\beta}$	10052.54	128	^{15}N	1833.35	32
3D CBCA(CO)NH	499.71	8082.44	$^{13}C^{\alpha,\beta}$	10052.54	118	^{15}N	1833.35	32
3D ^{1}H−^{15}N TOCSY HSQC	599.70	10999.59	^{15}N	2199.98	32	^{1}H	10999.59	128
3D ^{1}H−^{15}N NOESY HSQC	599.70	10999.59	^{1}H	10999.59	128	^{15}N	1833.35	32
3D HCCH-TOCSY	499.71	8082.44	^{1}H	8082.44	160	^{13}C	10052.78	64

[a] A total of 1024 complex points were collected in the ^{1}H dimension (d_1) of all experiments, except for 3D ^{15}N NOESY HSQC with 2048 complex points in d_1. [b] Details given in ref *39* for HSQC-based experiments, ref *63* for HNCA, HNCO, and HNCACB, ref *64* for CBCA(CO)NH, ref *65* for TOCSY and NOESY HSQC, and ref *66* for HCCH-TOCSY. [c] N_2 and N_3 are the number of complex points collected for the d_2 and d_3 dimensions, respectively.

time scale could not be monitored. Data sets were collected every 45 min for the first day and every 4−6 h thereafter for 3 days.

To assign ^{1}H and ^{15}N resonances of the His 56 imidazole ring in Adx^o and His 49 in Y51F Pdx^o, ^{1}H−^{15}N HSQC data sets were collected with the large spectral windows in the ^{15}N dimension using the Inova 600 MHz NMR. Spectral widths of 12001.2 Hz (^{1}H) and 20000 Hz (^{15}N) were used, with the carrier frequency for ^{15}N positioned at 158 ppm. A total of 256 × 1024 complex points were collected for each data set, with 256 and 170 scans per t_1 point for Adx^o and Y51F Pdx^o, respectively. The shorter acquisition time in the case of the Y51F mutant protein was dictated by decreased protein stability.

^{1}H resonances of Y51F Pdx^o were assigned using a combination of homonuclear NOESY and TOCSY data. A 2D homonuclear NOESY spectrum was obtained with a 70 ms NOE mixing time. Water suppression in the NOESY sequence was obtained using a gradient echo sequence. Two TOCSY experiments were performed, one with a 10 ms mixing time and one with 60 ms mixing time, to optimize direct and multiple step correlations, respectively. All experiments were performed on the Inova 500 MHz NMR, with the ^{1}H spectral width set at 8082.4 Hz. A total of 256 × 4096 complex points were collected, with 32 scans per t_1 point for NOESY. In the case of TOCSY experiments, a total of 256 × 2048 complex points were collected, with 32 scans per t_1 point.

All 2D NMR data sets were processed using the Felix 2.0 software package (Biosym). The Y51F Pdx^o NOESY and TOCSY data sets were processed using a 90° shifted sine bell squared window function together with multiplying the first point by 0.5, zero filling, and phase correcting spectra in both dimensions. A polynomial baseline straightening routine was applied routinely in the first dimension. Large spectral width data obtained for Adx^o and Y51F Pdx^o were processed using a 90° shifted sine bell window function, zero filling to increase the number of points by at least a factor of 2, in both, and phase correction only in the direct detected dimension. All data processing and analysis for amide H/D studies were performed using the Felix 2.0 software package (Biosym Techologies, San Diego, CA) operating on a Silicon Graphics O_2 work station. A 90° shifted sine bell window function was applied in both dimensions together with appropriate phase corrections. Peaks were identified on the basis of both previously published assignments (*33*) and assignments made as a part of this work. To extract information about the rate constants for amide H/D exchange, the time dependence of peak intensities was measured and fitted to a single exponential first-order rate equation.

For processing and analysis of results obtained by 3D triple resonance experiments, NMRPipe (*42*) was used for processing the data and NMRDraw (*43*) was applied for analysis of obtained spectra. A typical NMRPipe processing macro for ProteinPack-derived Varian 3D data sets is included in the Supporting Information.

Amide Proton Exchange Measurements for Oxidized and Reduced Forms of Adx. As noted above, the rates of amide proton exchange were measured for Adx^o and Adx^r by determining the rate of loss of correlations in ^{1}H,^{15}N HSQC spectra upon exchange of Adx into deuterated buffers. Amide H/D exchange was initiated by passage of the protonated sample through a short spin column packed with P2 (Bio-Rad) gel preequilibrated with the appropriate deuterated buffer. In the case of Adx^r, the sample was reduced prior to buffer exchange. Reduction of Adx was performed in a Coy anaerobic chamber under a 5% H_2/95% N_2 atmosphere by the addition of a small excess of a freshly prepared 1 M sodium dithionite solution in degassed 1 M Tris-HCl buffer (pH 7.4). The extent of reduction was followed visually, since the color of the protein changes from brown to ruby red. The Adx^r sample was placed in a susceptibility-matched NMR tube (Shigemi) and tightly sealed before being removed from the anaerobic chamber to prevent reoxidation. Other details of sample preparation for H/D exchange studies in this class of ferredoxin are published elsewhere (*41*).

RESULTS

Physical Characterization of Human Adx (4−114) Expressed from a Synthetic Gene. To gain insight into the physical properties of human Adx (4−114) expressed from a synthetic gene, we spectroscopically characterized the protein's pH and thermal stability. Four optical absorption maxima are observed for Adx^o with λ_{max} values at 275, 320, 415, and 455 nm. These values agree well with previously published spectra of human Adx^o. Upon reduction of Adx by $Na_2S_2O_4$, an additional absorption appears at 540 nm (as expected with the color change). These absorption maxima are due mainly to the charge transfer transitions resulting

from cysteinyl thiolate coordination of the iron atoms (*44*). Hence, their presence and intensities relative to the main aromatic residue absorption at 280 nm can be used to judge protein purity, metal cluster incorporation, and stability. We found that oxidized Adx (4−114) kept in 50 mM Tris-HCl, pH = 7.4, buffer at 4 °C remains folded over a period of ∼10 days. The half-life for human Adx^o (4−114) stability varies from 3 h at pH = 5 (50 mM imidazole hydrochloride buffer) to ∼3 days at pH = 8 (50 mM Tris-HCl buffer) at room temperature. A pronounced increase in stability of Adx^o occurs as one progresses from pH = 6 to pH = 7.

In the ^{1}H NMR spectrum of Adx, there are two signals that are shifted considerably downfield, with chemical shifts of 11.67 and 11.17 ppm. These signals are assigned to His 56 $N_{\delta 1}H$ and Ser 88 $O_\gamma H$, respectively (vide infra). Similar peaks are observed in the spectrum of Pdx and are assigned to the homologous His 49 $N_{\delta 1}H$ and Ser 82 $O_\gamma H$. These signals provide convenient markers for the complete and stable folding of the C-terminal lobe of the ferredoxin. We monitored the loss of these signals in human Adx^o (4−114), which occurs at T_{tr} = 50 ± 1 °C. This is similar to the observed behavior of bovine Adx (4−114), which has a transition temperature of T_{tr} = 50.9 °C (*45*).

^{1}H, ^{15}N, and ^{13}C NMR Assignments of Human Adx (4−114). Numerous NMR studies of Adx have been published over the last 10 years, including the pioneering homonuclear work of Miura and Ichikawa (*46*, *47*). Markley and co-workers have published extensively on this topic, including characterization of His resonances (*48*), redox-dependent chemical shift perturbations and sequential backbone assignments (*33*), and hyperfine-shifted resonances in the vicinity of the metal binding site, in both wild-type and mutant human Adx (*49*, *50*). Recently, Reuterjans and co-workers have published sequential backbone and side chain assignments for bovine Adx (*51*).

As part of the current effort, we have completed the ^{1}H, ^{15}N, and ^{13}C assignments for our construct of human Adx. The present work clears up some ambiguity regarding the resonance assignments of His 56 in Adx. This residue is conserved throughout the vertebrate ferredoxin family (with Tdx as a notable exception) and plays a critical role in the stability and dynamics of the C-terminal lobe (vide infra). Resonance assignments were not reported for His 56 either in the bovine Adx assignments (*51*) or in the backbone sequential assignments of human ferredoxin (Adx) (*33*). In their detailed multinuclear characterization of His resonances in human ferredoxin (Adx), Xia et al. assigned the $N_{\delta 1}$ of His 56 to the resonance at 238.5 ppm and the $N_{\epsilon 2}$ to a resonance at 169.8 ppm (*48*). However, the lack of complete through-bond correlations for the His 56 imidazole prevented the confirmation of these assignments. The crystal structure of bovine Adx^o places $N_{\delta 1}$ of His 56 (His 49 in Pdx) within hydrogen-bonding distance (3.1 Å) of the backbone carbonyl oxygen of Tyr 82, which is positionally homologous to Ala 76 in Pdx. NOEs observed to the $N_{\delta 1}H$ resonance in NMR spectra of human Adx are consistent with this conformation if the published imidazole ^{15}N assignments of His 56 (*48*) are reversed. ^{1}H−^{15}N HSQC spectra obtained with a large spectral width in the ^{15}N dimension and a large number of transients per t_1 point to increase sensitivity and obtain two-bond N−H couplings, confirms the one-bond correlation of the His 56 $N_{\delta 1}H$ at 11.67 ppm (^{1}H) to the ^{15}N resonance at 169.8 ppm, consistent with the crystallographic data for Adx. This data set also shows long-range correlations between a ^{1}H resonance at 7.26 ppm and both ^{15}N resonances in the imidazole ring (Figure 4) consistent with $^2J_{HN}$ coupling. As such, we assign this signal to the $C_{\epsilon 1}H$ resonance of His 56. A second ^{1}H signal at 6.93 ppm shows a long-range correlation only to the unprotonated ^{15}N at 238.5 ppm, assigning this signal to the $N_{\epsilon 2}$ and the proton signal at 6.93 to the $C_{\delta 2}H$ of His 56. As expected for an unprotonated imidazole, no $N_{\epsilon 2}H$ resonance is detected. Assignments for the conserved His in Adx, Pdx, and Y51F Pdx are listed in Table 2.

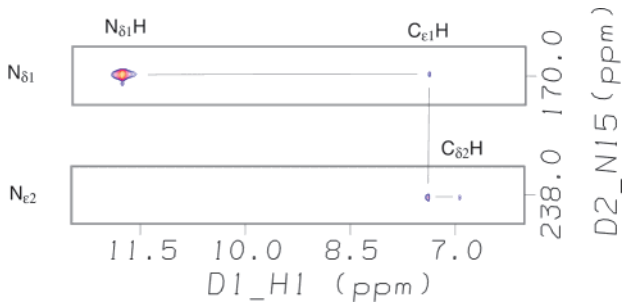

FIGURE 4: Portions of a ^{1}H,^{15}N HSQC spectrum of Adx^o (4−114) taken with a wide ^{15}N spectral width, showing the correlations between ^{1}H and ^{15}N resonances of the His 56 imidazole ring. The spectrum was obtained at 290 K and pH 7.4 at 500 MHz ^{1}H frequency.

Table 2: Assignments of Imidazole ^{15}N, ^{13}C, and ^{1}H Resonances from the Conserved His Residue in WT Pdx^o, Y51F Pdx^o, and Adx^o [a]

	$N_{\delta 1}$ (H)	$C_{\epsilon 1}$ (H)	$N_{\epsilon 2}$	$C_{\delta 2}$ (H)
WT Pdx His 49	170.0 (12.01)	136.3 (7.23)	246.8	122.8 (6.68)
Pdx Y51F His 49	166.7 (11.78)	(7.50)	243.4	
Adx His 56	166.8 (11.67)	135.7 (7.29)	240.0	124.2 (7.05)

[a] Assignments were made at 290 K, pH 7.4. ^{1}H shifts are shown in parentheses, preceded by heteronuclear shifts.

Table 3: Interresidue Nonsequential NOEs Involving His 56, Ile 58, and Ser 88 in Adx^o (4−114)

residue	NOE (residue)	NOE (atom)
His 56	His 56−Leu 84	$N_{\delta 1}H-C_\alpha H$
	His 56−Pro 108	$N_{\delta 1}H-C_\gamma H$
	His 56−Ile 58	$C_{\epsilon 1}H-C_\gamma H$
	His 56−Leu 84	$C_{\epsilon 1}H$−NH, $C_{\epsilon 1}H-C_\alpha H$
	His 56−Ser 88	$C_{\epsilon 1}H-O_\gamma H$
Ile 58	Ile 58−Phe 59	$C_\alpha H-C_\alpha H$, $C_\alpha H-C_\beta H$
	Ile 58−Ser 88	C_αH−NH, $C_\alpha H-C_\alpha H$, $C_\gamma H-O_\gamma H$
	Ile 58−Arg 106	$C_\alpha H-C_\beta H$
Ser 88	Phe 59−Ser 88	NH−NH
	Leu 84−Ser 88	$C_\alpha H-O_\gamma H$, $C_\gamma H-O_\gamma H$, $C_\delta H-O_\gamma H$
	Thr 85−Ser 88	NH−NH, NH−C_αH, NH−O_γH, $O_\gamma H-C_\alpha H$, $O_\gamma H-O_\gamma H$
	Asp 86−Ser 88	C_αH−NH

The NOEs observed in human Adx (4−114) are consistent with the hydrogen-bonding network observed in the crystal structure of truncated bovine Adx (11) (see Table 3). The $O_\gamma H$ proton of Ser 88 is detected in Adx (11.2 ppm) and exhibits a strong NOE to the $C_{\epsilon 1}H$ proton of His 56, as expected if this proton hydrogen bonds to the $N_{\epsilon 2}$ of His 56. The absence of an $N_{\epsilon 2}H$ resonance is consistent with the $N_{\epsilon 2}$ being a hydrogen bond acceptor from the $O_\gamma H$ proton of Ser 88. Both the slow-exchange nature of the $O_\gamma H$ resonance of

Ser 88 and the downfield shift (OH protons usually occur between 0.5 and 5 ppm) confirm that this proton is involved in a strong hydrogen-bonding interaction.

Mutations at the Conserved His 49 in Pdx and Physical Characterization of Y51F Pdx. Pdx also contains a hydrogen bond network in its C-terminal lobe. On the basis of the refined solution structure of Pdx^o, His 49 $N_{\epsilon 2}$ acts as a hydrogen bond acceptor to the phenolic proton $O_\eta H$ from Tyr 51, and O_η of Tyr 51 acts as a hydrogen bond acceptor from Ser 82 $O_\gamma H$ (*14*). The importance of His 49 in this network was tested by site-directed mutagenesis. Two mutants of Pdx were prepared, one in which His 49 was replaced by Phe and one that duplicates the His−Arg substitution observed in Tdx. Phe in this position is unable to make any hydrogen bonds but is expected to maintain any hydrophobic contacts made by His in the WT protein, whereas Arg should allow hydrogen bonding but decrease hydrophobic interactions. Both H49F and H49R Pdx mutants were expressed at normal efficiency as judged by SDS−PAGE of crude cell lysate. However, neither mutant was expressed as a holoprotein (i.e., with an intact Fe−S cluster) nor could either holoprotein be isolated and purified from reconstitutions performed under normal conditions. It is clear from these results that the stability of Pdx is severely compromised by the replacement of His 49 with these other residues. It is interesting to note that Adx, at least, can tolerate these same mutations at the corresponding position (His 56) since the H56R and H56N mutants of bovine Adx have been reported to reconstitute with a metal cluster and to be at least marginally stable (*52*).

Another member of the proposed hydrogen-bonding network in Pdx, Tyr 51, was also mutated to Phe. Again, it was expected that this mutation would maintain the hydrophobic contacts of residue 51 while removing the hydrogen-bonding ability. The Y51F Pdx mutant was expressed primarily as an apoprotein, although a holoprotein appeared to be present in some amount, based on the slight brown color of cell-free extracts. The optical spectrum of reconstituted Y51F Pdx^o is similar to that of WT Pdx^o, showing a distinct peak at 325 nm and a faint shoulders at 415 and 455 nm. Loss of the Fe−S cluster as a function of pH and temperature was monitored by the disappearance of the 415 and 455 nm bands. It was determined that the half-life of Y51F Pdx^o in degassed buffers ranges from ~30 min at pH = 5 to ~10 h at pH = 8, at room temperature. As with Adx, there is a relatively large change in acid stability as going from pH = 6 to pH = 7.

The functional activities of the Y51F Pdx mutant and WT protein were compared using the complete reconstituted CYP101 camphor hydroxylase system. Turnover was measured by following the camphor- and O_2-dependent decrease of the NADH absorbance at 340 nm. It was determined that Y51F Pdx retains about 33% activity of WT Pdx.

Comparison of WT and Y51F Pdx Structures. Homonuclear ^{1}H 2D NOESY and TOCSY data were used to assign some of the resonances of interest in Y51F Pdx^o. Some of these assignments are listed in Table 4 together with the corresponding assignments for WT Pdx. Nonsequential NOEs that characterize the C-terminal lobe of Y51F are shown in Table 5. Chemical shift differences between Y51F and WT Pdx are not large, indicating that the mutant does not experience significant structural perturbations. As expected, the largest chemical shift differences are observed for residue 51, although the imidazole protons of His 49 undergo some small chemical shift changes as well. One of the signature peaks for complete folding of Pdx in the ^{1}H NMR spectrum is the Ser 82 $O_\gamma H$, which is homologous with Ser 88 in Adx, and appears at 10.10 ppm. This resonance was assigned previously via coupling to the $C_\beta H_2$ of Ser 82 (*53*, *54*). Serine hydroxyl protons are not usually detectable as discrete resonances, since they tend to rapidly exchange with solvent. As for the Ser 88 $O_\gamma H$ in Adx, the severe downfield shift indicates that the Ser 82 $O_\gamma H$ group is involved in a strong hydrogen bond, probably to the O_η of Tyr 51 (vide supra). One obvious difference between Y51F and WT Pdx is the absence of the Ser 82 $O_\gamma H$ peak in the Y51F ^{1}H spectrum, indicating that this proton is now at fast exchange with solvent, as expected if the Y51 $O_\eta H$ is the hydrogen bond acceptor in WT Pdx. However, the relatively small perturbations to the His 49 imidazole resonances suggest that this residue is still involved in multiple hydrogen bonds even in the Y51F mutant. One possibility is that the cavity vacated by the $O_\eta H$ group of Tyr 51 in Y51F Pdx is occupied by a water molecule. This water molecule would be able to form the hydrogen bond to the $N_\epsilon H$ of His 49

Table 4: ^{1}H Resonance Assignments for Y51F Pdx^o Compared with Corresponding Assignments for WT Pdx^o [a]

resonance type	chemical shift in WT Pdx^o	chemical shift in Y51F Pdx^o
His 49 $N_{\delta 1}H$	12.01	11.77
His 49 $C_{\epsilon 1}H$	7.23	7.47
His 49 $C_{\delta 2}H$	6.68	6.73
Tyr 51/Phe 51 $C_\alpha H$	4.96	5.03
Tyr 51/Phe 51 $C_\beta H$	2.69, 2.62	2.79, 2.71
Tyr 51/Phe 51 $C_\delta H$	6.63	6.78
Tyr 51/Phe 51 $C_\epsilon H$	6.65	7.21
Tyr 51/Phe 51 $C_z H$		7.11
Ala 76 NH	7.62	7.56
Lys 79 NH	9.71	9.60
Ser 82 NH	7.98	7.92
Ser 82 $C_\alpha H$	5.02	5.02
Ser 82 $C_\beta H$	3.98, 3.90	3.98, 3.92
Ser 82 $O_\gamma H$	10.10	
Arg 83 NH	9.37	9.32
Trp 106 $C_{\epsilon 1}H$	10.04	9.96

[a] Assignments were made at 290 K, pH 7.4.

Table 5: Interresidue Nonsequential NOEs Involving His 49, Phe 51, Ala 76, and Ser 82 in Y51F Pdx^o

residue	NOE (residue)	NOE (atom)
His 49	His 49−Phe 51	$C_{\epsilon 1}H-C_{\epsilon 1}H$
	His 49−Ala 76	$C_{\epsilon 1}H-C_\beta H$
	His 49−Leu 78	$C_{\epsilon 1}H-C_\alpha H$
Phe 51	Phe 51−Lys 79	$C_{\epsilon 1}H-C_\delta H$, $C_\epsilon H-NH$, $C_\delta H-C_\beta H$
	Phe 51−Asn 81	$C_\alpha H-C_\delta H$, $C_\beta H-C_\delta H$
	Phe 51−Ser 82	$C_\alpha H-NH$, $C_\beta H-C_\alpha H$, $C_\delta H-NH$, $C_\delta H-C_\alpha H$, $C_\epsilon H-C_\alpha H$
	Phe 51−Arg 83	$C_\alpha H-NH$, $C_\delta H-C_\delta H$
	Phe 51−Asp 100	$NH-C_\alpha H$
	Phe 51−Pro 102	$NH-C_\alpha H$, $C_\epsilon H-C_\beta H$, $C_z H-C_\beta H$
Ala 76	Val 74−Ala 76	$C_\gamma H-NH$
	Ala 76−Leu 78	$NH-C_\alpha H$
	Ala 76−Pro 102	$C_\beta H-C_\beta H$
	Ala 76−Arg 104	$C_\beta H-C_\alpha H$, $C_\beta H-C_\epsilon H$, $C_\alpha H-C_\beta H$
Ser 82	Leu 71−Ser 82	$C_\delta H-C_\beta H$
	Leu 78−Ser 82	$C_\delta H-C_\alpha H$, $C_\alpha H-NH$, $C_\delta H-C_\beta H$
	Lys 79−Ser 82	$NH-NH$, $NH-C_\beta H$

Table 6: Interresidue Nonsequential NOEs Involving Arg 49, Glu 51, Glu 76, and Thr 82 in Tdx[o]

residue	NOE (residue)	NOE (atom)
Arg 49	Arg49−Leu 71	$N_\epsilon H-C_\delta H_3$
	Arg 49−Thr 82	$C_\epsilon H-C_\gamma H$
	Arg 49−Thr 82	$N_\epsilon H-C_\gamma H$
	Arg49−Pro102	$C_\alpha H-C_\alpha H$
Glu 51	Glu 51−Thr 82	$C_\alpha H-C_\alpha H$, $C_\alpha H-C_\gamma H$
	Glu 51−Arg 83	$C_\alpha H-NH$
	Glu 51−Arg 100	NH−NH, $NH-C_\alpha H$
	Glu 51−Val 101	$NH-C_\alpha H$
	Glu 51−Pro 102	$NH-C_\delta H_2$
Glu 76	Thr 74−Glu 76	NH−NH, $C_\alpha H-NH$, $C_\beta H-NH$, $C_\gamma H-NH$
	Glu 76−Met 78	$C_\beta H-NH$
Thr 82	Ile 52−Thr 82	NH−NH, $NH-C_\alpha H$
	Val 57−Thr 82	$C_\gamma H_{1,2}-NH$
	Met 78−Thr 82	$C_\alpha H-C_\gamma H_1$
	Thr 79−Thr 82	$NH-C_\beta H$, NH−NH, $NH-C_\gamma H_1$
	Ile 80−Thr 82	$C_\alpha H-NH$

that is provided by the $O_\eta H$ of Tyr 51 in WT Pdx. NOEs are observed from the bulk water signal to the aromatic $C_\epsilon H$ protons of Phe 51, providing support this proposal.

The C-Terminal Lobe of Tdx. The solution structure of Tdx[o] was determined using NMR methods (*15*). Unlike either Adx or Pdx, there is a paucity of nonsequential NOE restraints for the C-terminal region of Tdx, particularly involving Arg 49. Several NOEs are observed that indicate interaction between the side chains of Arg 49 and Thr 82 (see Table 6). However, their lack of a signal for the Thr 82 $O_\gamma H$ similar to those for the Ser 88 $O_\gamma H$ in Adx and Ser 82 $O_\gamma H$ in Pdx suggests that any hydrogen bond involving the Thr 82 $O_\gamma H$ is not as strong in Tdx as in the other two ferredoxins. However, NOEs observed to the Arg 83 side chain, which forms a conserved internal salt bridge with Glu 67 in Pdx (corresponding to Glu 76//Arg 89 in Adx), are consistent with this salt bridge being present in Tdx as well.

Reduction Potential Measurements. Since vertebrate-type ferredoxins function as electron carriers, their activity is closely related to the value of their redox potentials. Therefore, we obtained relative values for the redox potentials for all of the proteins discussed here via the photochemical dye method. The reduction potential for human Adx (4−114) was determined by redox titration to be 28 mV more negative than that of WT Pdx, making it more difficult to reduce than Pdx. This is consistent with literature values that place the difference in redox potentials between WT Pdx and bovine Adx at 35 mV, with Adx being more negative (*55*, *56*).

The reduction potential of Y51F Pdx is 24 mV more positive than that of WT Pdx, which was reported to be −240 mV, at room temperature and pH = 7.4 (*55*). Hence, the mutation either stabilizes the reduced form of Pdx or destabilizes the oxidized form. Tdx is even easier to reduce than Y51F Pdx, having a reduction potential 44 mV more positive than that of WT Pdx. All of these ferredoxins are still sufficiently strong reducing agents that they can reduce camphor-bound CYP101 (reduction potential of −170 mV) (*57*).

Comparison of Local Dynamics in Pdx, Adx, and Tdx via H/D Exchange Measurements. Amide proton exchange rates provide a measure of local solvent accessibility as well as local backbone dynamics within a folded protein. In the current work, we have completed a survey of the differences between protein dynamics of oxidized and reduced forms of vertebrate-type ferredoxins. Results of such comparisons for Pdx and Tdx have been reported previously (*15*, *41*). We now report rates of H/D exchange for residues in both oxidized and reduced human Adx (4−114). Peak intensities in 2D $^1H-^{15}N$ HSQC spectra obtained as a function of exchange time were fit to a first-order exponential decay function in order to extract rate constants. Results for residues that show marked differences between oxidized and reduced forms of Adx//Pdx//Tdx are shown in Table 7. Since the lag time between initial buffer exchange and the first HSQC spectrum was approximately 30 min, exchange rate constants faster than $\sim 3 \times 10^{-3}$ s^{-1} could not be measured, and those exchange processes are marked as "fast" in Table 7. Also, since the data collection was stopped after 3 days, all those exchange processes with half-lives longer than that were not determined and marked as "slow" in Table 7. Xia et al. previously published qualitative H/D exchange data for oxidized full-length human Adx, noting those residues for which backbone amide protons show slow exchange (*33*). Our results are in agreement with theirs. In addition, we have quantitatively determined H/D exchange rates in both oxidized and reduced forms of human Adx (4−114). A comprehensive list of measured rate constants and residue-specific ratios of rate constants in Adx[o] and Adx[r] is provided in the Supporting Information.

Table 7: Comparison of H/D Exchange Rate Constant Ratios for Adx, Pdx, and Tdx for Residues That Are Most Affected by Oxidation State Changes, Given as Ratios of k_{ox}/k_{red}[a]

Adx		Pdx		Tdx	
residue no.	k_{ox}/k_{red}	residue no.	k_{ox}/k_{red}	residue no.	k_{ox}/k_{red}
20	**17.35**	14	fast[b]	14	fast[b]
32	fast	26	>**34**	26	0.62
34	slow[c]	28	**5.4**	28	3.76
36	0.64	30	>**12**	30	fast
38	**8.67**	32	0.97	32	2.76
60	1.15	53	>**55**	53	0.66
71	>**72.02**	64	1.9	64	fast
77	N/A[d]	70	N/A	70	**7.56**
78	N/A	71	N/A	71	**6.83**
79	>**63.54**	72	1.01	72	fast
80	fast	74	>**52**	74	fast
82	>**37.61**	76	>**16**	76	fast
85	fast	79	**14**	79	fast
88	3.26	82	>**12**	82	1.28
89	4.83	83	slow	83	**6.19**
101	**26.17**	95	N/A	95	0.75
110	fast	104	>**8.4**	104	fast

[a] Residues with $k_{ox}/k_{red} > 5$ are shown in boldface. Together with those, k_{ox}/k_{red} for the corresponding residues in the other two proteins are also provided for comparison reasons. [b] Refers to the case when H/D exchange is a process with a half-lifetime shorter than 30 min for both oxidized and reduced forms, making those rate constants inaccessible by our measuring method. [c] Refers to exchange processes with half-lives longer than 1.5 days for both oxidized and reduced forms. [d] N/A refers to cases where NH resonances of either oxidized/reduced or both are unassigned due to paramagnetic broadening.

As can be seen in Table 7, all three proteins, Adx, Pdx, and Tdx, contain two redox-responsive regions. One is the region just preceding the iron−sulfur binding loop in the N-terminal lobe. Residues that show the greatest dynamic sensitivity to redox changes in this region include Ala 26, Val 28, and Asn 30 in Pdx, Ala 27, Thr 28, and Val 32 in Tdx, and Thr 20 and Leu 38 in Adx. Pdx shows the most

pronounced redox-dependent differences in this region, while Tdx shows the least. The second region includes residues in the C-terminal lobe, including Asn 53, Val 74, Ala 76, Lys 79, Ser 82, and Arg 104 in Pdx, Leu 70, Leu 71, and Arg 83 in Tdx, and Thr 71, Asp 79, Tyr 82, and Asp 101 in Adx. Again, Tdx is the least affected by changes in oxidation state. However, redox-dependent differences in Adx in this region are, in general, larger than those observed in Pdx in the C-terminal lobe.

DISCUSSION

Local Environment of the C-Terminal Cluster and Comparison between Pdx, Tdx, and Adx. In all three of the structures being compared, Adx, Pdx, and Tdx, the compact C-terminal lobes are formed by a combination of polar and hydrophobic interactions. (For comparison purposes, when residues are to be referred to in all three proteins simultaneously, the residue names and numbers will be written in the order Adx//Pdx//Tdx.) While a number of conserved hydrophobic residues contribute to the formation of the C-terminal lobe, including Leu 78//Leu71//Leu71, Leu 84//Leu 78//Met 78, and Leu 90//Leu 84//Leu 84, the region is distinctive in that a significant number of internal polar interactions are present as well. All three proteins contain homologous internal salt bridges that essentially span their C-terminal lobes. This salt bridge involves a carboxylate on the long helix (Glu 74//Glu 67//Glu 67) and a conserved Arg residue (Arg 89//Arg 83//Arg 83) that immediately follows a tight turn in all three structures (see Figure 1). Mutation of Glu 74 results in destabilization of human Adx, as expected if this salt bridge is important for stability of the cluster region (*26*). Similar observations have been made for bovine Adx, (*2*) and a similar salt bridge is seen in *E. coli* ferredoxin (see ref *16*).

The structures of Adx and Pdx clearly indicate why the conserved His 56//His 49 is important: the hydrogen-bonding network it forms links the backbone of the protein near the proposed docking site with cytochrome P450 with the rest of the C-terminal cluster. Mutation of His 56 in Adx results in proteins that are significantly less stable than WT, although the H56R, H56T, and H56Q mutations in bovine Adx are reported to be sufficiently stable that activity assays could be performed with them (*2*, *52*). Our mutations of His 49 in Pdx to Phe and Arg resulted in proteins that, although overexpressed in *E. coli* (as indicated by gel electrophoresis), could not be reconstituted to form stable holoproteins.

The situation of His 49 that is observed in Pdx is similar but not identical to that observed for His 56 in Adx. The chemical shifts of ^{1}H, ^{15}N, and ^{13}C resonances for the imidazole of His 49 in Pdx correspond closely to those of His 56 in Adx (Table 2). The $N_{\delta 1}H$ of His 49 shows NOEs to the side chain resonances of Val 74 and the NH and $C_{\beta}H_3$ of Ala 76. This is consistent with a hydrogen bond between the carbonyl of Ala 76 and the $N_{d1}H$ of His 49, which would be precisely homologous to the hydrogen bond between His 56 $N_{\delta 1}H$ and the carbonyl of Tyr 82 in Adx. However, the distance between Ser 82 $O_{\gamma}H$ and the His 49 $N_{\epsilon 2}$ is too great for a direct hydrogen-bonding interaction. Instead, the $O_{\eta}H$ of Tyr 51 lies approximately between the $O_{\gamma}H$ of Ser 82 and the $N_{\epsilon 2}$ of His 49 and acts as part of a hydrogen-bonding relay, with the $O_{\eta}H$ proton of Tyr 51 hydrogen bonding to the $N_{\epsilon 2}$ of His 49 and the $O_{\gamma}H$ of Ser 82 hydrogen bonded to the O_{η} of Tyr 51.

In Tdx the situation is different from that in either Adx or Pdx. More of the polar interactions stabilizing the C-terminal lobe are ionic: instead of His, the conserved basic residue is Arg (Arg 49). The side chain of Arg 49 is adjacent to the acidic side chain of Glu 51, which occupies an internal position homologous that of Tyr 51 (Pdx) and Ile 58 (Adx). As such, the His 49−Tyr 51 hydrogen bond observed in Pdx is likely to be an ionic interaction in Tdx (although no direct proof of this exists). Furthermore, the hydroxyl proton of Thr 82 (Ser in Pdx and Adx) is not observed at slow exchange in Tdx, suggesting that whatever interactions might involve this residue, they do not stabilize the OH group against exchange to the same extent that the hydrogen bonds to Ser 88//Ser 82 do in Adx and Pdx. The Arg 49 guanidinium group can form hydrogen bonds with backbone carbonyls in a manner similar to that of His 49//His 56, although, again, lack of NOE evidence precludes any firm conclusions in this regard. What is clear is that protein dynamics in the C-terminal lobe of Tdx is less strongly coupled to the oxidation state of the metal cluster than in either Adx or Pdx. We attribute this to two factors. First, the Arg side chain is more flexible than the His side chain and, so, is less capable of transmitting mechanical perturbations that occur in the metal binding loop to the C-terminal lobe. Second, the ionic interactions in Tdx will be less directional than the hydrogen-bonding networks of either Pdx or Adx and, hence, able to adjust to changes in conformation of one member of an ion pair without significant changes in the other.

Origin of Redox-Dependent Dynamics in Ferredoxins. It is now well established that all of the vertebrate ferredoxins exhibit redox-dependent dynamic behavior. We have found that amide proton exchange (reflecting millisecond to kilosecond time scales) is significantly slower in Pdx^{r} than in Pdx^{o}, particularly in the C-terminal lobe. Other workers have shown that Pdx exhibits redox dependence of local dynamics at intermediate (nanosecond to millisecond) time scales as well, again with Pdx^{r} being less dynamic than Pdx^{o} (*58*). Although standard NMR methods cannot directly probe protein dynamics near the metal cluster due to paramagnetic broadening, an EPR/ESEEM study of Adx confirms that amide exchange in the immediate vicinity of the metal cluster is highly oxidation state dependent, with reduced Adx showing essentially no H/D exchange (*59*). From the results presented here, we can conclude that, as is true for Pdx, Adx^{o} is more dynamic than Adx^{r}. Furthermore, the same region (the C-terminal lobe) is most affected by change in the oxidation state. In a recent publication (*4*), we underscored the critical role that the polypeptide of the Fe−S cluster binding loop (Gly 37−Cys 48) plays in modulating dynamics as a function of oxidation state in Pdx. A particular mutation in the metal cluster binding loop, G40N, increases the barriers to conformational exchange in Pdx^{o} sufficiently so that many ^{1}H resonances that are somewhat broadened by conformational exchange in WT Pdx^{o} are broadened to obscurity or split into multiple signals in G40N Pdx^{o}. Upon reduction, both G40N and WT Pdx give rise to essentially identical spectra, indicating that reduction of the metal cluster "tightens" the structure and that little or no conformational freedom is available to the metal binding loop in either G40N

or WT Pdx^r. We attributed this behavior to the strengthening (shortening) of hydrogen bonds between the sulfur atoms of the metal cluster and the amide NH groups of the surrounding polypeptide due to the increased negative charge on the cluster in Pdx^r. On the basis of our interpretation of paramagnetic $^{13}C(O)$ and ^{15}N shift changes in the metal cluster binding loop upon reduction, we hypothesized that this strengthening of hydrogen bonds upon reduction causes an increased "pucker" in the polypeptide of the metal cluster binding loop (*4*). It is expected that this "puckering" will result in a mechanical perturbation that is transmitted to the rest of the protein via the polypeptide backbone and side chains.

Role of the Conserved Basic Residue His 56//His 49//Arg 49 and Associated Hydrogen-Bonding Network in Protein Stability and Redox-Dependent Dynamics. One question that we seek to answer in the current work is the role of particular structural features of the C-terminal lobe in transmitting the proposed redox-dependent mechanical perturbations from the metal binding site to other regions of the protein. Whereas residues most affected by reduction in the N-terminal lobe of these ferredoxins are either sequentially or spatially adjacent to the metal binding loop, most of the residues in the C-terminal lobes that are strongly affected by oxidation state changes are somewhat remote from the metal cluster. As such, a mechanism for transmitting redox-dependent perturbations to this region of the protein must be sought.

On the basis of evidence described here and elsewhere, the conserved basic residue His 56//His 49//Arg 49 is a critical player in this mechanism. Occupying as it does the position immediately following the third cysteinyl ligand of the Fe_2S_2 cluster in the metal binding loop of Pdx, this residue is ideally situated to respond to conformational and/or dynamic changes in the metal binding loop that result from changes in oxidation state. The CXTCH (X = A, S) motif is common to many ferredoxins and open reading frames expected to code for ferredoxins. A casual search of the SWISS−PROT database yields at least 30 sequences with significant homology to Pdx, almost all of which contain the CXTCH sequence (see Figure 2). These sequences are found in a wide variety of organisms, including bacteria, archaea, yeast, and vertebrates. In a few cases (such as Tdx), the histidine residue is replaced by arginine. Prior to the availability of structural data on this class of ferredoxin, it was postulated that the conserved histidine interacted with the metal center to modulate redox potential or to provide a pathway for electron transfer. However, our early NMR investigations of Pdx showed that the imidazole of His 49 is further than 10 Å from the metal center, as it does not experience significant paramagnetic broadening (*53*). Nevertheless, the imidazole of His 49 does have some unusual properties. It exhibits an abnormally low pK_a, as it does not protonate to form imidazolium over the pH range at which Pdx is stable (between pH ~9 and pH ~6.5). The unprotonated $N_{\epsilon 2}$ nitrogen exhibits a chemical shift of 247 ppm, near the extreme for any diamagnetic His $N_{\epsilon 2}$ nitrogen (*60*). The behavior of His 56 in Adx is nearly identical. Xia et al. indicated that His 56 $N_{\delta 1}H$ has a low pK_a (below 5), and we have assigned the $N_{\delta 1}H$ at 11.67 ppm and $N_{\epsilon 2}$ at 240 ppm. In the crystal structure of truncated Adx^o, the $N_{\delta 1}H$ of His 56 is hydrogen bonded to the backbone carbonyl oxygen of Tyr 82 (*11*). NMR data alone cannot confirm the precise acceptor of the hydrogen bond from His 49 $N_{\delta 1}H$ in Pdx. However, multiple NOEs are observed between the imidazole $N_{\delta 1}H$ and $C_{\epsilon 1}H$ protons of His 49 and resonances of Ala 76 (which is structurally homologous with Tyr 82 in Adx) and Glu 77 (*14*). Furthermore, the chemical shifts of Ala 76 are among the most sensitive to redox changes at the metal center (*54*). All of these data suggest that the carbonyl of Ala 76 is in fact the acceptor of the hydrogen bond with the $N_{\delta 1}H$ of His 49 in Pdx.

Another unusual feature shared by Pdx and Adx is that a resonance can be assigned to the Ser 88//Ser 82 $O_\gamma H$ in both proteins. In Pdx^o, the $O_\gamma H$ resonance occurs at 10.10 ppm and in Adx^o at 11.17 ppm. The fact that we can detect the Ser $O_\gamma H$ in both proteins indicates that in both cases the $O_\gamma H$ group is involved in a strong hydrogen bond that moves the chemical shift downfield and slows exchange with solvent. A similar resonance for Thr 82 $O_\gamma H$ in Tdx could not be identified, suggesting that the homologous hydrogen bond is not present or at least is not as strong in Tdx. On the basis of NOEs and the crystal structure of Adx, the hydrogen bond acceptor for the Ser 88//Ser 82 $O_\gamma H$ in Adx is His 56 $N_{\epsilon 2}$ and in Pdx is Tyr 51 O_η. NMR results for the Y51F Pdx mutant support the assumption that the Tyr 51 O_η is the hydrogen bond acceptor for Ser 82 $O_\gamma H$, since in the mutant protein a resonance of Ser 82 $O_\gamma H$ is not observed. The decreased stability of the Y51F mutant relative to that of WT Pdx indicates that the hydrogen bonds to Tyr 51 $O_\gamma H$ are important in stabilizing the fold of the C-terminal lobe.

CONCLUSIONS

The C-terminal lobes of vertebrate ferredoxins share a common feature in that they are compact regions of structure that are stabilized more by ionic and polar interactions than by hydrophobic interactions. In all three ferredoxins discussed here, an internal salt bridge extends between a conserved Glu and Arg (Glu 74−Arg 89 in Adx) and contributes significantly to protein stability, at least in the case of Adx (*61*). In both Pdx and Adx, a conserved His residue (His 56 in Adx) takes part in forming a network of hydrogen bonds that extends from a backbone carbonyl (Tyr 82 in Adx) to a conserved Ser OH group (Ser 88 in Adx). In Adx, this is a direct interaction between the Ser 88 OH and the unprotonated His 56 $N_{\epsilon 2}$, whereas in Pdx, the phenolic OH of Tyr 51 (positionally homologous to Ile 58 in Adx) forms an intermediary hydrogen bond between the conserved His imidazole and the conserved serine hydroxyl. Together, these polar interactions link the major structural features of the C-terminal lobe, the long helix, the β-sheet and turn, and the loop from the helix to the turn.

The location of the conserved His at the C-terminal end of the metal binding loop puts it in an ideal position to sense redox-dependent changes in conformation and dynamics at the metal binding site and then to transmit those changes to the C-terminal lobe. We previously proposed that, upon reduction of the metal center (with the concomitant increase in the negative charge on the cluster), there is a strengthening (shortening) of hydrogen bonds between the sulfur ligands of the metal cluster and the surrounding polypeptide NH group (*4*). The net result is a contraction of the polypeptide that forms the metal binding loop around the metal cluster in Pdx^r. This contraction would have the effect of pulling

the ends of the metal binding loop in. The His 49 side chain would be pulled along with this motion, and the C-terminal hydrogen-bonding network would be pulled in as well, resulting in a more compact, less dynamic C-terminal lobe in Pdx^r.

It is clear that a similar process takes place in Adx upon reduction. In fact, the overall larger effects of reduction upon amide exchange rates observed in Adx relative to Pdx suggest that the shorter hydrogen bond network in the C-terminal lobe of Adx transmits conformational and dynamic information from the metal center more efficiently than the corresponding network in Pdx. Conversely, the replacement of His by the conformationally more flexible Arg in Tdx weakens the mechanical linkage between the metal center and the C-terminal lobe of that protein, making the effects of reduction upon local dynamics in the C-terminal lobe of Tdx in general smaller than in either Pdx or Adx. It is possible that less directional ionic interactions, as opposed to hydrogen bonding, predominate in the interactions of Arg 49 with Glu 51, weakening further the mechanical linkage between the metal center and the C-terminal lobe of Tdx.

It is worth noting that the trend in reduction potentials measured for the wild-type ferredoxins discussed here tracks with the sensitivity of local dynamics in the C-terminal lobe (as measured by amide H/D exchange) to reduction of the metal center. Adx, which shows the greatest linkage between the metal center and the C-terminal lobe, is also the most difficult to reduce. Pdx is somewhat less sensitive to metal center oxidation state and has an intermediate reduction potential, while Tdx is the least sensitive to oxidation state changes and also is the most readily reduced of the three ferredoxins. The temperature dependence of the reduction potential of Pdx^o shows that Pdx^o is entropically favored (*62*), as would be expected if protein dynamics has a role to play in modulation of reduction potential in this class of ferredoxin.

SUPPORTING INFORMATION AVAILABLE

A complete description of the synthesis of the human Adx (4−114) gene, oligonucleotides used in the synthesis of mutants, rate constants for amide exchange in Adx, complete amide exchange ratios for Pdx, Tdx, and Adx as a function of oxidation state, and a typical NMRPipe macro used for processing triple-resonance Varian ProteinPack NMR data, plus a Nernst plot of the Y51F Pdx redox determination, the UV−visible spectrum of Y51F Pdx^o, HSQC spectra of Adx before and after H/D exchange, and MALDI-TOF mass spectra of WT and Y51F Pdx. This information is available free of charge via the Internet at http://pubs.acs.org. The ^1H, ^{15}N, and ^{13}C resonance assignments of human Adx^o (4−114) have been deposited in the BMRB database (Accession Number 5337).

REFERENCES

1. Stephens, P. J., Jollie, D. R., and Warshel, A. (1996) *Chem. Rev. 96*, 2491−2513.
2. Grinberg, A. V., Hannemann, F., Schiffler, B., Muller, J., Heinemann, U., and Bernhardt, R. (2000) *Proteins: Struct., Funct., Genet. 40*, 590−612.
3. Overington, J. P. (1992) *Curr. Opin. Struct. Biol. 2*, 394−401.
4. Pochapsky, T. C., Kostic, M., Jain, N., and Pejchal, R. (2001) *Biochemistry 40*, 5602−5614.
5. Rypniewski, W. R., Breiter, D. R., Benning, M. M., Wesenberg, G., Oh, B. H., Markley, J. L., Rayment, I., and Holden, H. M. (1991) *Biochemistry 30*, 4126−4131.
6. Jacobson, B. L., Chae, Y. K., Markley, J. L., Rayment, I., and Holden, H. M. (1993) *Biochemistry 32*, 6788−6793.
7. Tsukihara, T., Fukuyama, K., Mizushima, M., Harioka, T., Kusunoki, M., Katsube, Y., Hase, T., and Matsubara, H. (1990) *J. Mol. Biol. 216*, 399−410.
8. Ikemizu, S., Bando, M., Sato, T., Morimoto, Y., Tsukihara, T., and Fukuyama, K. (1994) *Acta Crystallogr. D 50*, 167−174.
9. Bes, M. T., Parisini, E., Inda, L. A., Saraiva, L. M., Peleato, M. L., and Sheldrick, G. M. (1999) *Struct. Folding Des. 7*, 1201−1211.
10. Sussman, J. L., Shoham, M., Harel, M., and Yonath, A. (1984) *Acta Crystallogr. A 40*, C40.
11. Muller, A., Muller, J. J., Muller, Y. A., Uhlmann, H., Bernhardt, R., and Heinemann, U. (1998) *Structure 6*, 269−280.
12. Pikuleva, I. A., Tesh, K., Waterman, M. R., and Kim, Y. C. (2000) *Arch. Biochem. Biophys. 373*, 44−55.
13. Pochapsky, T. C., Ye, X. M., Ratnaswamy, G., and Lyons, T. A. (1994) *Biochemistry 33*, 6424−6432.
14. Pochapsky, T. C., Jain, N. U., Kuti, M., Lyons, T. A., and Heymont, J. (1999) *Biochemistry 38*, 4681−4690.
15. Mo, H. P., Pochapsky, S. S., and Pochapsky, T. C. (1999) *Biochemistry 38*, 5666−5675.
16. Kakuta, Y., Horio, T., Takahashi, Y., and Fukuyama, K. (2001) *Biochemistry 40*, 11007−11012.
17. Takahashi, Y., and Nakamura, M. (1999) *J. Biochem. 126*, 917−926.
18. Bernhardt, R., Muller, A., Uhlmann, H., Grinberg, A., Muller, J. J., and Heinemann, U. (1998) *Endocr. Res. 24*, 531−539.
19. Mueller, E. J., Loida, P. J., and Sligar, S. G. (1995) in *Cytochrome P450: Structure, Function and Biochemistry* (Ortiz de Montellano, P., Ed.) pp 83−124, Plenum Press, New York.
20. Peterson, J. A., Lu, J. Y., Geisselsoder, J., Grahamlorence, S., Carmona, C., Witney, F., and Lorence, M. C. (1992) *J. Biol. Chem. 267*, 14193−14203.
21. Fruetel, J. A., Mackman, R. L., Peterson, J. A., and Demontellano, P. R. O. (1994) *J. Biol. Chem. 269*, 28815−28821.
22. Lipscomb, J. D., Sligar, S. G., Namtvedt, M. J., and Gunsalus, I. C. (1976) *J. Biol. Chem. 251*, 1116−1124.
23. Holden, M. J., Mayhew, M., and Vilker, V. L. (1998) *Abstr. Pap.−Am. Chem. Soc. 216*, 049-BIOL.
24. Holden, M. J., Mayhew, M., Bunk, D., Roitberg, A., and Vilker, V. L. (1997) *FASEB J. 11*, P108.
25. Coghlan, V. M., and Vickery, L. E. (1992) *J. Biol. Chem. 267*, 8932−8935.
26. Coghlan, V. M., and Vickery, L. E. (1991) *J. Biol. Chem. 266*, 18606−18612.
27. Nakamura, K., Horiuchi, T., Yasukochi, T., Sekimizu, K., Hara, T., and Sagara, Y. (1994) *Biochim. Biophys. Acta 1207*, 40−48.
28. Berhardt, R., Kraft, R., Uhlmann, H., and Beckert, V. (1994) *J. Protein Chem. 13*, 482−483.
29. Davies, M. D., and Sligar, S. G. (1992) *Biochemistry 31*, 11383−11389.
30. Pochapsky, T. C., Lyons, T. A., Kazanis, S., Arakaki, T., and Ratnaswamy, G. (1996) *Biochimie 78*, 723−733.
31. Roitberg, A. (1997) *Abstr. Pap.−Am. Chem. Soc. 213*, 200-BIOT.
32. Roitberg, A. E., Holden, M. J., Mayhew, M. P., Kurnikov, I. V., Beratan, D. N., and Vilker, V. L. (1998) *J. Am. Chem. Soc. 120*, 8927−8932.
33. Xia, B., Volkman, B. F., and Markley, J. L. (1998) *Biochemistry 37*, 3965−3973.
34. Uhlmann, H., Kraft, R., and Bernhardt, R. (1994) *J. Biol. Chem. 269*, 22557−22564.
35. Rosenberg, A. H., Lade, B. N., Chui, D. S., Lin, S. W., Dunn, J. J., and Studier, F. W. (1987) *Gene 56*, 125−135.

36. Sligar, S. G., and Gunsalus, I. C. (1976) *Proc. Natl. Acad. Sci. U.S.A. 73*, 1078−1082.
37. Wishart, D. S., Bigam, C. G., Holm, A., Hodges, R. S., and Sykes, B. D. (1995) *J. Biomol. NMR 5*, 332.
38. Cavanagh, J., Palmer, A. G., Wright, P. E., and Rance, M. (1991) *J. Magn. Reson. 91*, 429−436.
39. Kay, L. E., Keifer, P., and Saarinen, T. (1992) *J. Am. Chem. Soc. 114*, 10663−10665.
40. Shaka, A. J., Barker, P. B., and Freeman, R. (0000) *J. Magn. Reson. 52*, 335−338.
41. Lyons, T. A., Ratnaswamy, G., and Pochapsky, T. C. (1996) *Protein Sci. 5*, 627−639.
42. Delaglio, F., Grzesiek, S., Vuister, G. W., Zhu, G., Pfeifer, J., and Bax, A. (1995) *J. Biomol. NMR 6*, 277−293.
43. Johnson, B. A., and Blevins, R. A. (1994) *J. Biomol. NMR 4*, 603−614.
44. Sow, T. C., Pedersen, M. V., Christensen, H. E. M., and Ooi, B. L. (1996) *Biochem. Biophys. Res. Commun. 223*, 360−364.
45. Burova, T. V., Beckert, V., Uhlmann, H., Ristau, O., Bernhardt, R., and Pfeil, W. (1996) *Protein Sci. 5*, 1890−1897.
46. Miura, S., and Ichikawa, Y. (1991) *Eur. J. Biochem. 197*, 747−757.
47. Miura, S., and Ichikawa, Y. (1991) *J. Biol. Chem. 266*, 6252−6258.
48. Xia, B., Cheng, H., Skjeldal, L., Coghlan, V. M., Vickery, L. E., and Markley, J. L. (1995) *Biochemistry 34*, 180−187.
49. Xia, B., Jenk, D., Lemaster, D. M., Westler, W. M., and Markley, J. L. (2000) *Arch. Biochem. Biophys. 373*, 328−334.
50. Skjeldal, L., Markley, J. L., Coghlan, V. M., and Vickery, L. E. (1991) *Biochemistry 30*, 9078−9083.
51. Weiss, R., Brachais, L., Lohr, F., Hartleib, J., Bernhardt, R., and Ruterjans, H. (2000) *J. Biomol. NMR 17*, 355−356.
52. Beckert, V., Schrauber, H., Bernhardt, R., Vandijk, A. A., Kakoschke, C., and Wray, V. (1995) *Eur. J. Biochem. 231*, 226−235.
53. Ye, X. M., Pochapsky, T. C., and Pochapsky, S. S. (1992) *Biochemistry 31*, 1961−1968.
54. Pochapsky, T. C., Ratnaswamy, G., and Patera, A. (1994) *Biochemistry 33*, 6433−6441.
55. Wilson, G. S., Tsibris, J. C. M., and Gunsalus, I. C. (1973) *J. Biol. Chem. 248*, 6059−6061.
56. Huang, Y. Y., and Kimura, T. (1983) *Anal. Biochem. 133*, 385−393.
57. Sligar, S. G. (1976) *Biochemistry 15*, 5399−5406.
58. Sari, N., Holden, M. J., Mayhew, M. P., Vilker, V. L., and Coxon, B. (1999) *Biochemistry 38*, 9862−9871.
59. Orme-Johnson, N. R., Mims, W. B., Orme-Johnson, W. H., Bartsch, M. A., Cusanovich, M. A., and Peisach, J. (1983) *Biochim. Biophys. Acta 748*, 68−72.
60. Farr, E. A., Seavey, B. R., Conti, A. M., Westler, W. M., and Markley, J. L. (1993) *J. Cell. Biochem.*, 252.
61. Brandt, M. E., and Vickery, L. E. (1993) *J. Biol. Chem. 268*, 17126−17130.
62. Reipa, V., Holden, M. J., Mayhew, M. P., and Vilker, V. L. (2000) *Biochim. Biophys. Acta 1459*, 1−9.
63. Muhandiram, D. R., and Kay, L. E. (1994) *J. Magn. Reson., Ser. B 103*, 203−216.
64. Grzesiek, S., and Bax, A. (1992) *J. Am. Chem. Soc. 114*, 6291−6293.
65. Zhang, O. W., Kay, L. E., Olivier, J. P., and Formankay, J. D. (1994) *J. Biomol. NMR 4*, 845−858.
66. Saltler, M., Schwendinger, M. G., Schleucher, J., and Griesinger, C. (1995) *J. Biomol. NMR 6*, 11−22.
67. Koradi, R., Billeter, M., and Wüthrich, K. (1996) *J. Mol. Graphics 14*, 51−55.
68. Thompson, J. D., Higgins, D. G., and Gibson, T. J. (1994) *Nucleic Acids Res. 22*, 4673−4680.

BI0200256